electronic reprint

Journal of
Applied Crystallography
ISSN 0021-8898
Editor: **Gernot Kostorz**

Correction for counting losses in X-ray diffractometry

T. Ida and Y. Iwata

Journal of
Applied Crystallography
ISSN 0021-8898

Received 10 September 2004
Accepted 21 February 2005

Correction for counting losses in X-ray diffractometry

T. Ida* and Y. Iwata

Ceramics Research Laboratory, Nagoya Institute of Technology, Asahigaoka, Tajimi, Gifu 507-0071, Japan. Correspondence e-mail: ida.takashi@nitech.ac.jp

Non-extended and extended dead-time models, a pulse-height analyser (PHA) windowing model, and a model intermediate between the non-extended and extended models for losses in counting methods are compared. The validities of the methods are examined by application to the analysis of powder diffraction peak intensity profiles measured by a foil method. The intermediate model including parameters for the dead-time and degree of extension can reproduce both the non-extended and the extended models and also intermediate dependence between the two models. A convenient approximate formula for the intermediate model, the maximum relative deviation of which is 0.0003, is also proposed. The determination of the parameters and a correction for the measured intensities can easily be achieved by applying the approximate model, because it provides simple formulae for the correction function expressed as a combination of elementary functions. Experimental and analytical methods for precise evaluation of the parameters to specify the counting losses are also presented. Systematic deviations of the observed dependence from the non-extended and extended dead-time models have been detected by the precise analyses of experimental data, while the PHA windowing model, intermediate model and its approximation have reproduced the observed dependence within the experimental errors.

1. Introduction

The counting method for evaluating diffracted beam intensity is widely adopted in X-ray diffraction measurements. Detection methods with counting devices are often more favourable for precise structure analyses because of the intrinsically linear sensitivity and well defined nature of the statistical errors, in contrast to methods with time-integrating detectors, such as an imaging plate (IP). However, the effect of counting losses due to the dead-time of the detector or the finite response time of the detection circuits may cause serious systematic errors in the intensities observed by the counting method, especially at high count rates.

Counting losses are usually modelled by a non-extended dead-time model or an extended dead-time model (Quintana, 1991). In the non-extended dead-time model, it is assumed that an event causes dead-time τ, but the following events during the time τ do not extend the dead-time. In the extended dead-time model, the same event would extend the length of the dead-time by τ starting at the arrival time of the uncounted event.

The throughput function of the non-extended dead-time model (Müller, 1973) is given by

$$n = f_{\text{non–ex}}(r; \tau) = r/(1 + r\tau), \tag{1}$$

where n is the observed count rate, r is the true count rate and τ is the dead-time. The solution of the above equation is given by

$$r = f^{-1}_{\text{non–ex}}(n; \tau) = n/(1 - n\tau), \tag{2}$$

which can immediately be applied to correct the counting losses.

The counting losses in a realistic detection system are more likely to be modelled by the extended dead-time model (Omote, 1990; Reed, 1972), given by

$$n = f_{\text{ex}}(r; \tau) = r\exp(-r\tau). \tag{3}$$

Cousins (1994) has proposed the following formula for synchrotron X-ray sources,

$$n = T_{\text{b}}^{-1}\exp(-mrT_{\text{b}})[1 - \exp(-rT_{\text{b}})], \tag{4}$$

where T_{b} is the bunch interval and m is the largest integer not greater than τ/T_{b}. For the usual case of $\tau \gg T_{\text{b}}$, equation (4) can simply be reduced to the extended dead-time model.

The actual losses in the counting method are affected by the time structure of the X-ray source and the operating characteristics of the detector/amplifier system. When a pulse-height analyser (PHA) or a single-channel analyser (SCA) is used to reduce the effect of electrical noise, stray light or higher-order harmonics of the monochromated incident beam,

the settings for the PHA windowing may also affect the loss of counts (Cousins, 1994). Therefore, experimental evaluation of counting losses seems more practical than fully theoretical prediction requiring many parameters to be determined.

Quintana (1991) has proposed a practical analytical method to evaluate the dead-time parameter in the extended model, from the experimental data measured by the foil method of Chipman (1969), which can easily be performed with most X-ray diffraction setups. However, the accuracy of the correction will be restricted if the actual counting losses deviate from the exact extended model.

The present study is intended to establish an improved method to determine the dependence of the observed count rate on the true count rate from the data measured by Chipman's foil method, and to correct the counting losses in the observed diffraction intensity data, allowing deviation from the non-extended or extended dead-time models. A convenient formula for correction, which can be used for intermediate dependence between non-extended and extended dead-time models, is proposed.

2. Models for counting losses

2.1. PHA windowing model

When a pulse-height analyser is used to count the pulses, the output count rate will be affected by the allowed pile-up level L (Cousins, 1994). If all the input pulses are assumed to have the same rectangular shape, the output count rate through the PHA will be given by

$$n = r\exp(-2r\tau_{\rm w})\sum_{l=0}^{L-1}(r\tau_{\rm w})^l/l!, \tag{5}$$

where $\tau_{\rm w}$ is the width of a pulse and L is the allowed pile-up level normalized to the single-pulse-height level. The derivation of the formula is given in Appendix *A*. The above formula can readily be extended for non-integer values of L by the equation

$$n = r\exp(-r\tau_{\rm w})\,{\rm Q}(L, r\tau_{\rm w}), \tag{6}$$

where the function ${\rm Q}(\nu, z)$ is the Legendre incomplete gamma function of the second kind, defined by

$${\rm Q}(\nu, z) \equiv \int_z^\infty t^{\nu-1}\exp(-t)\,{\rm d}t\left[\int_0^\infty t^{\nu-1}\exp(-t)\,{\rm d}t\right]^{-1}. \tag{7}$$

Since the throughput function is specified by two continuous parameters, $\tau_{\rm w}$ and L in equation (6), a usual nonlinear curve fitting method can be applied to determine those parameters from the experimental data. The profiles of the throughput function on variation of the allowed pile-up level L are shown in Fig. 1.

When the allowed pile-up level is equal to the single-pulse-height level (L = 1), the detected count rate is given by

$$n = r\exp(-2r\tau_{\rm w}), \tag{8}$$

which is identical to the extended dead-time model for $\tau = 2\tau_{\rm w}$. In the $L \to \infty$ limit, the detected count rate is identical to the extended model for $\tau = \tau_{\rm w}$ given by

$$n = r\exp(-r\tau_{\rm w}). \tag{9}$$

The derivatives of the function at the origin (r = 0) show singularities for some values of L as follows,

$$({\rm d}n/{\rm d}r)_0 = 1, \tag{10}$$

$$({\rm d}^2n/{\rm d}r^2)_0 = \begin{cases} -\infty & (L<1) \\ -4\tau_{\rm w} & (L=1) \\ -2\tau_{\rm w} & (L>1) \end{cases}, \tag{11}$$

$$({\rm d}^3n/{\rm d}r^3)_0 = \begin{cases} +\infty & (L<1) \\ 12\tau_{\rm w}^2 & (L=1) \\ -\infty & (1<L<2) \\ 0 & (L=2) \\ 3\tau_{\rm w}^2 & (L>2) \end{cases}, \tag{12}$$

while the non-extended and extended dead-time models have no singularities at the origin. The first, second and third derivatives of the non-extended and extended dead-time models are given by

$$f'_{\rm non\text{–}ex}(0;\tau) = 1, \tag{13}$$

$$f''_{\rm non\text{–}ex}(0;\tau) = -2\tau, \tag{14}$$

$$f'''_{\rm non\text{–}ex}(0;\tau) = 6\tau^2, \tag{15}$$

and

$$f'_{\rm ex}(0;\tau) = 1, \tag{16}$$

$$f''_{\rm ex}(0;\tau) = -2\tau, \tag{17}$$

$$f'''_{\rm ex}(0;\tau) = 3\tau^2. \tag{18}$$

The throughput of the PHA looks very much like the extended dead-time model, as can be seen in Fig. 1, even though there exist slight deviations for $L \neq 1$. Comparison of the first few derivatives at the origin suggests that the deviation is in the direction of the non-extended model for $0 < L < 1$ and in the opposite direction for $1 < L$.

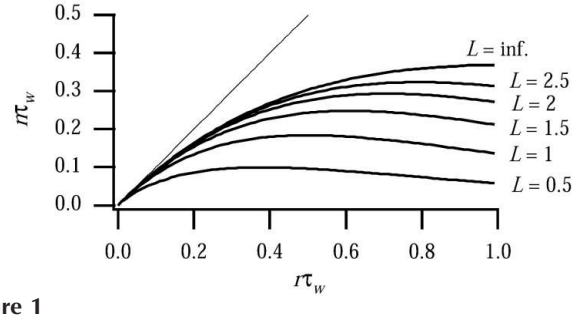

Figure 1
Throughput predicted by a simple model for the effect of PHA windowing.

2.2. Intermediate model between non-extended and extended models

An intermediate model between the non-extended and extended dead-time models can be constructed by synthesizing the two functions as follows:

$$n = f_{\rm ex}[f_{\rm non\text{–}ex}(r; \tau_1); \tau_2], \tag{19}$$

where τ_1 and τ_2 are the dead-time parameters for the non-extended and extended components of the function, respectively. The first, second and third derivatives of the above function at the origin are given by

$$(\mathrm{d}n/\mathrm{d}r)_0 = 1,$$

$$(\mathrm{d}^2n/\mathrm{d}r^2)_0 = -2(\tau_1 + \tau_2),$$

$$(\mathrm{d}^3n/\mathrm{d}r^3)_0 = 6\tau_1^2 + 12\tau_1\tau_2 + 3\tau_2^2,$$

while the derivatives of the component functions are given by equations (13)–(18). It will be convenient to substitute the total dead-time parameter τ and the degree of extension ρ for the parameters τ_1 and τ_2, *via* the equations

$$\tau \equiv \tau_1 + \tau_2, \tag{20}$$

$$\rho \equiv \tau_2^2/\tau^2, \tag{21}$$

which gives the formula

$$f_{\rm intermediate}(r; \tau, \rho) = r[1 + (1 - \rho^{1/2})r\tau]^{-1} \times \exp\{-\rho^{1/2}r\tau[1 + (1 - \rho^{1/2})r\tau]^{-1}\}. \tag{22}$$

The formula exactly gives the non-extended and extended dead-time dependences for $\rho = 0$ and $\rho = 1$, respectively. The value of the third derivative of the throughput function at the origin is linearly varied by changing the parameter ρ from 0 to 1.

Even if a sufficiently high count rate is not experimentally available, or the statistical errors of the experimental data are not small enough to estimate the precise value for the degree of extension ρ, the total dead-time parameter τ can be estimated more safely, because it is determined by the initial curvature of the throughput. The parameter ρ can easily be treated as a fixed parameter, if necessary.

2.3. Approximation for intermediate model

In order to evaluate the true count rate r from the observed count rate n, the inverse function of the throughput function is needed, while both the PHA windowing and the intermediate models for counting losses described in §§2.1 and 2.2 lack simple formulae for the inverse functions. Although the solutions can be evaluated numerically by iterative calculation based on Newton's method (Cousins, 1994), the codings for Newton's method are often annoying, because the accuracy, stability and efficiency of the iterative calculation strongly depend on the initial guess of the solution, maximum iteration times and criteria for convergence.

In this section, an approximate formula, which has a simple expression of its inverse function, is proposed. The scheme for constructing the approximate formula is described in Appendix *B*.

Table 1
Values of the first four derivatives of the counting loss model functions at the origin.

Order	$f(x; \tau, 0) = f_{\rm non\text{–}ex}(x; \tau)$	$f(x; \tau, 1)$	$f_{\rm ex}(x; \tau)$
1	1	1	1
2	-2τ	-2τ	-2τ
3	$6\tau^2$	$3\tau^2$	$3\tau^2$
4	$-24\tau^3$	$-3.973\tau^3$	$-4\tau^3$

The approximate model is given by the equations

$$n = f(r;\ \tau, \rho) = \begin{cases} t_2^{-1}[\exp(-r't_2) - \exp(-2r't_2)] & [t_2 \neq 0] \\ r' & [t_2 = 0] \end{cases}, \tag{23}$$

$$r' = r/(1 + rt_1), \tag{24}$$

$$t_1 = \tau - 3t_2/2, \tag{25}$$

$$t_2 = (6\rho/13)^{1/2}\tau, \tag{26}$$

where ρ is a parameter corresponding to the degree of dead-time extension, similarly to the exact intermediate model in the preceding section.

This model is identical to the non-extended model for $\rho = 0$, that is,

$$f(r; \tau, 0) \equiv f_{\rm non\text{–}ex}(r; \tau), \tag{27}$$

and also approximates the extended model for $\rho = 1$ reasonably well,

$$f(r; \tau, 1) \simeq f_{\rm ex}(r; \tau). \tag{28}$$

The maximum deviation of $f(r; \tau, 1)$ from $f_{\rm ex}(r; \tau)$ in the range $0 \leq r \leq \tau^{-1}$ is 0.0003 relative to the value of $f_{\rm ex}(r; \tau)$ at $r = \tau^{-1}$, which is smaller than the statistical errors predicted for data counts up to 10^7.

The values of the derivatives of the functions $f(r; \tau, \rho)$, $f_{\rm non\text{–}ex}(r; \tau)$ and $f_{\rm ex}(r; \tau)$ at the origin are listed in Table 1.

The inverse function of the model function $f(x; \tau, \rho)$ is given by the equations

$$r = f^{-1}(n; \tau, \rho) = r'/(1 - r't_1), \tag{29}$$

$$r' = \begin{cases} -t_2^{-1}\ln\{[1 + (1 - 4nt_2)^{1/2}]/2\} & [t_2 \neq 0] \\ n & [t_2 = 0] \end{cases}, \tag{30}$$

where t_1 and t_2 are related to τ and ρ by equations (25) and (26).

3. Estimation of parameters

3.1. Experimental

The experimental procedures referred to as Chipman's (1969) foil method were applied to estimate the parameters in the counting loss models. The 2θ scan intensity profiles for the 003 reflection of mica powder (NIST, SRM675) were

measured with a high-resolution powder diffractometer (Toraya *et al.*, 1996) on beamline BL4B$_2$ at the Photon Factory (PF) in Tsukuba. The 2θ angle was measured with an encoder (Heidenhain RON-806) at each measurement step. The specimen was rotated about its surface normal during the measurements. One measurement was made with an aluminium foil absorber inserted in the beam path, and the second measurement was made without the foil. A high-voltage/PHA unit (Rigaku 5320 C1) was used to count the signal pulses. The baseline and width of the window of the PHA were set to 0.5 and 2, respectively, relative to the first peak position in the PHA differential curve. Changes in intensity caused by the decay of the ring current were calibrated by monitoring the intensity of the incident beam.

3.2. Analytical method

3.2.1. Preliminary analysis. Since the 2θ angles of the two measurements did not strictly coincide, intensities expected for the common 2θ angles with equal intervals were calculated by sampling intensity values from the curves drawn by a cubic spline interpolation between the observed data points. The first intensity data, $\{y_{1j}\}$, were calculated from the data $\{2\theta_{1j}\}$ and $\{Y_{1j}\}$ measured with the foil absorber, and the second set of data, $\{y_{2j}\}$, were calculated from the data $\{2\theta_{2j}\}$ and $\{Y_{2j}\}$ measured without the foil.

Fig. 2 shows the observed intensity profiles for the first (attenuated) and second (unattenuated) measurements. Both data were measured at 0.001° steps in 2θ. The reduction in the observed intensities near the peak top in the second measurement clearly shows that it is heavily affected by losses in the counting method.

The interpolated second set of intensity data $\{y_{2j}\}$ are plotted *versus* the interpolated first intensity data $\{y_{1j}\}$ in Fig. 3. Firstly, the dependence was modelled by the extended dead-time model, applying the fitting function

$$y'_{1j} = f_{\rm ex}[a^{-1} f_{\rm ex}^{-1}(y_{1j};\, \tau);\, \tau], \tag{31}$$

where a is the transmittance of the foil.

The transmittance a and dead-time parameter τ were determined by applying a nonlinear least-squares optimization to the observed dependence of $\{y_{2j}\}$ on $\{y_{1j}\}$, to minimize the quantity

$$\chi^2 = \sum_j (y_{2j} - y'_{1j})^2 / \sigma_j^2, \tag{32}$$

where σ_j is the estimated error for each data point. The errors were estimated by assuming counting statistics for the second intensity data set $\{y_{2j}\}$, given by

$$\sigma_j^2 = (y_{2j}/T_{2j})^{1/2}, \tag{33}$$

where T_{2j} is the measurement time for the second data set at each step, for the preliminary evaluation of the parameters. The inverse function $f_{\rm ex}^{-1}(x;\tau)$ was calculated by a Newton method, with the initial guess of the solution as $x/(1-x\tau)$, ten-times iteration and no criteria for convergence.

The result of the preliminary fitting to the data with the extended dead-time model is also shown in Fig. 3. Systematic deviation showing a hysteresis-like behaviour is found in the difference plot, which suggests a slight constant shift of the abscissa between the two measurements.

3.2.2. Correction of shift. In order to evaluate the shift of the abscissa precisely, the correlation between the preliminarily modified values for the first data y'_{1j}, which were calculated with the optimized values of a and τ, and the second intensity data set y_{2j} was examined. The correlation was calculated by

$$c_k = \sum_{j=0}^{n-k-1} y'_{1j} y_{2,j+k}, \tag{34}$$

where n is the total number of data points. A periodicity of

$$c_{k+n} = c_k \tag{35}$$

is assumed.

Fig. 4 shows the correlation curve and results of fitting with a Lorentzian function:

$$f_{\rm Lor}(\Delta 2\theta) = b + (S/\pi w)[1 + (\Delta 2\theta - \Delta 2\theta_0)^2/w^2]^{-1}, \tag{36}$$

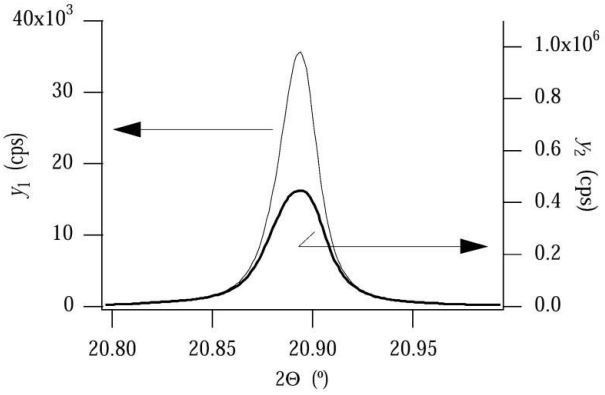

Figure 2
The peak profiles of the mica 003 reflection measured at the Photon Factory. The profile measured with a foil absorber is shown as a thin line, and that measured without the foil is shown as a thick line.

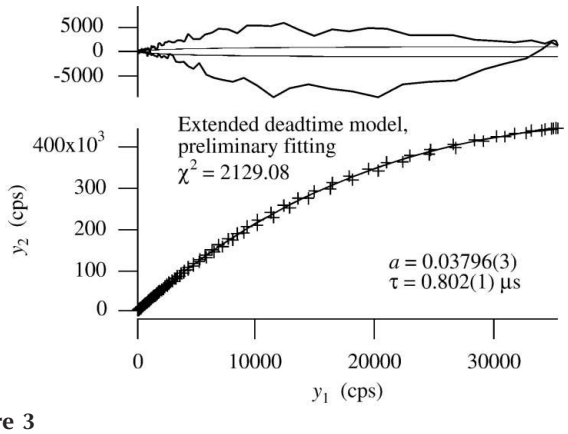

Figure 3
The result of a preliminary fitting with the extended dead-time model to the data shown in Fig. 2. The experimental data are shown as crosses and the optimized curve is shown as a solid line in the lower part of the figure. The difference is shown as a thick line and the estimated errors ($\pm\sigma$) are shown as thin lines in the upper part.

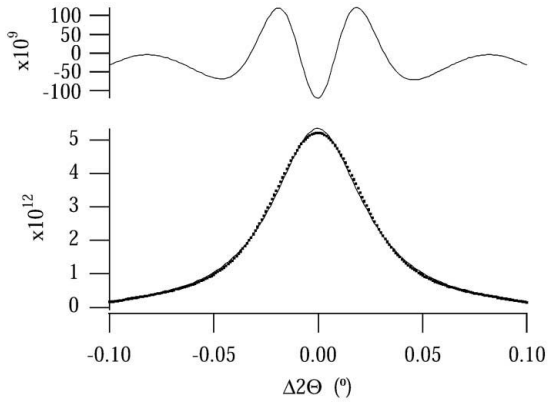

Figure 4
Correlation curve to evaluate the slight shift. The experimental correlations are shown as dots and the optimized curve is shown as a thin solid line in the lower part. The upper part shows the difference plot.

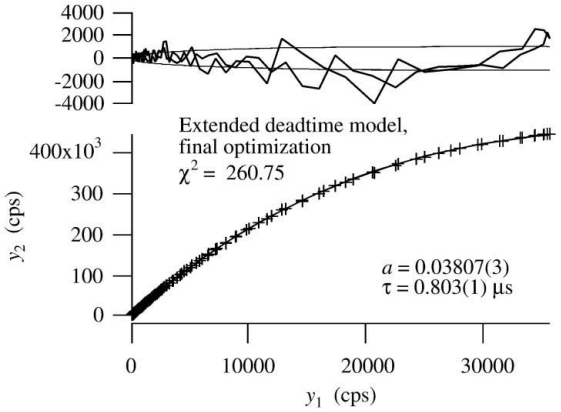

Figure 5
The result of the final optimization with the extended dead-time model using the data shown in Fig. 2. Data are represented as described in the caption of Fig. 3.

where b is the background, S is the intensity, $\Delta 2\theta_0$ is the peak shift and w is the half width at half-maximum of the Lorentzian function.

The optimized value for the peak shift is $\Delta 2\theta_0 = -0.00025^\circ$, which means that the second set of data are shifted by 0.00025° to the lower-angle side as compared with the first data set.

The shift-corrected intensity data for the second measurement, $\{y'_{2j}\}$, were then created by applying a cubic spline interpolation to the data set shifted by $\Delta 2\theta_0$, $\{2\theta_{2j} + \Delta 2\theta_0\}$ and $\{Y_{2j}\}$.

3.2.3. Final optimization. Final optimization was conducted to minimize the quantity

$$\chi^2 = \sum_j (y'_{2j} - y'_{1j})^2/(\sigma'_j)^2, \qquad (37)$$

where σ'_j is the estimated error for each data point. The statistical errors in the first measurement are also taken into account in the final optimization, applying the equation

$$\sigma'_j = [y'_{2j}(T_{2j}^{-1} + T_{1j}^{-1} y'_{1j}/y_{1j})]^{1/2}, \qquad (38)$$

where T_{1j} and T_{2j} are the measurement time at each step for the first and second data set, respectively.

Table 2
Results of optimization for different counting loss models.

a is the transmittance of the foil, τ is the dead-time, L is the allowed pile-up level and ρ is the degree of dead-time extension.

Model	a	τ (μs)	ρ or L	χ^2
Extended	0.03807 (3)	0.803 (1)		260.8
Non-extended	0.03639 (3)	1.196 (2)		3548.4
PHA-windowing	0.03768 (6)	0.364 (4)	L = 0.900 (11)	194.2
Intermediate	0.03784 (4)	0.842 (5)	ρ = 0.872 (15)	187.8
Approximate	0.03784 (4)	0.842 (5)	ρ = 0.872 (15)	187.8

Fig. 5 shows the result of the final fitting analysis with the extended dead-time model, where the shift correction of -0.00025° is applied to the data shown in Fig. 2. The statistical errors corresponding to ± 1 standard deviation are shown as thin lines in the upper part of Fig. 5. The difference plot, shown as thick lines in the upper part of Fig. 5, suggests slight systematic deviation of the observed dependence from that predicted by the extended dead-time model. It should be noted that such slight systematic deviation could not be detected without the shift correction of 0.00025°, which is much smaller than the measurement step of 0.001°.

3.2.4. Comparison of models for counting losses. The non-extended dead-time model, the PHA-windowing model in §2.1, the intermediate model in §2.2 and the approximate intermediate model in §2.3 were also applied to the data analysed in the preceding section. The results for the four models are shown in Figs. 6–9 and are listed in Table 2.

The non-extended dead-time model poorly fits the observed dependence (Fig. 6). However, the tendency of the systematic deviation is found to be in the opposite direction to that of the extended dead-time model shown in Fig. 5. This result suggests that the observed dependence has a character intermediate between the non-extended and extended dead-time models.

When the allowed pile-up level L is treated as an adjustable parameter, the PHA-windowing model can fit the observed dependence reasonably well (Fig. 7). There remain no significant systematic deviations in the difference plot of Fig. 7. However, the optimized value L = 0.900 (11) is inconsistent with the PHA settings applied for the measurement, where the baseline and width of the window are set to 0.5 and 2 relative to the first peak position in the PHA differential curve. There seems no theoretical evidence to suggest any advantage of the simple PHA-windowing model for counting losses. The optimized value of L less than 1 means that the deviation from the extended dead-time model (L = 1) is in the direction of the non-extended model, as discussed in §2.1.

The intermediate model gives slightly better fits (smaller χ^2) to the observed dependence, as shown in Fig. 8. The optimized value ρ = 0.872 (15) shows that the experimental dependence is mainly reproduced by the extended dead-time model (ρ = 1), but the contribution of the non-extended dead-time model (ρ = 0) is not negligible.

Application of the approximate intermediate model, described in §2.3, gives no difference from the exact intermediate model within the experimental errors (Fig. 9), except that the codings are easier and the computation time needed is

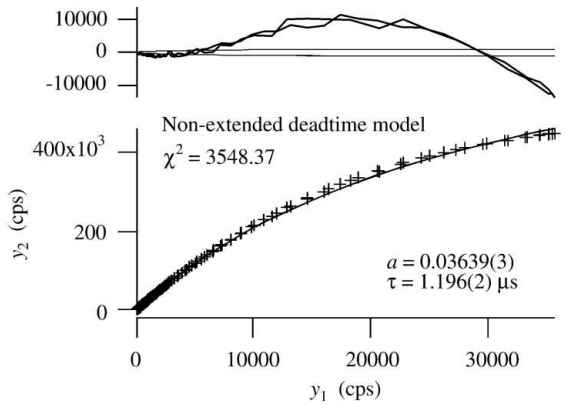

Figure 6
The result of the final optimization with the non-extended dead-time model using the data shown in Fig. 2. Data are represented as described in the caption of Fig. 3.

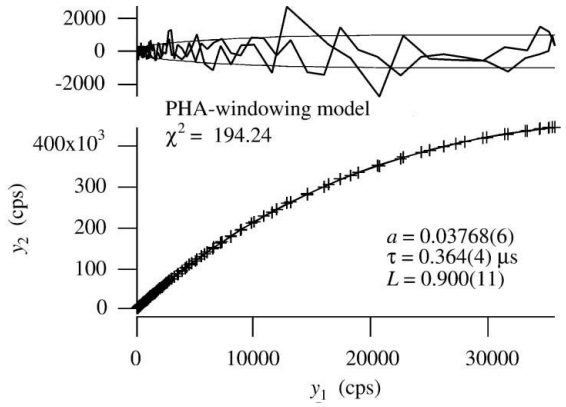

Figure 7
The result of the final optimization with the PHA-windowing model using the data shown in Fig. 2. Data are represented as described in the caption of Fig. 3.

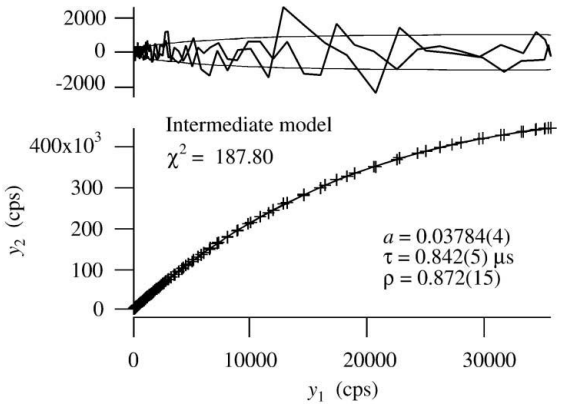

Figure 8
The result of the final optimization with the intermediate model using the data shown in Fig. 2. Data are represented as described in the caption of Fig. 3.

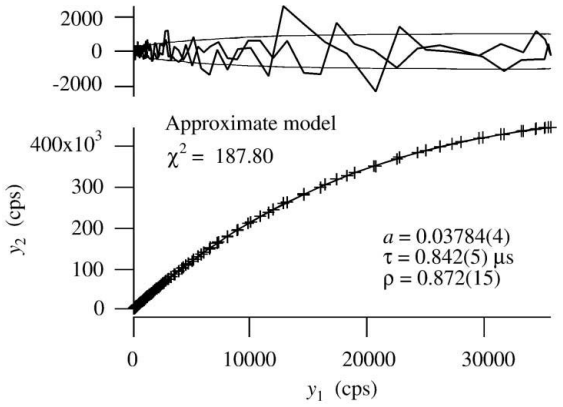

Figure 9
The result of the final fitting with the approximation for the intermediate model using the data shown in Fig. 2. Data are represented as described in the caption of Fig. 3.

shorter in the approximate model, where no iterative calculation is needed for evaluation of the inverse function. It should be noted that the efficiency in the evaluation of the inverse function will become more significant when the model is applied to correct the counting losses in experimental powder X-ray diffraction intensity data with many data points.

4. Conclusion

Non-extended and extended dead-time models, a PHA-windowing model, an intermediate model, and an approximate intermediate model for counting losses have been applied to high-precision analyses of experimental diffraction peak intensity profiles measured by a foil method. The deviations of the experimental dependence from the convenient approximate model are within the experimental errors. Both the optimization of the parameters and corrections for counting losses can easily be achieved by applying the approximate model, because the exact solution of its inverse function is expressed by a combination of elementary functions.

APPENDIX *A*
Derivation of a counting loss model for PHA windowing

It is assumed that the input pulses have a common rectangular shape with width τ_w. The Poisson distribution for the number of pulses N in a fixed time T is given by

$$f_P(N, T) = (rT)^N \exp(-rT)/N!, \qquad (39)$$

where r is the average count rate.

When the PHA is set to allow only single-height pulses ($L = 1$) and to reject any pile-up peaks, an input pulse will be detected only when the interval from the last pulse and the interval to the next pulse are both longer than the pulse width τ_w. The probability that each pulse is detected is given by $\exp(-2r\tau_w)$, because the probability that no pulse occurs within the period τ_w is given by $f_P(0, \tau_w) = \exp(-r\tau_w)$. The output count rate is then expected to be $r\exp(-2r\tau_w)$.

For the case of $L = 2$, the following logic is applied. (i) A pulse is temporarily detected when the interval from the last pulse is longer than τ_w. (ii) The temporarily detected pulse is cancelled when two or more pulses occur within the following

period τ_w, or fixed otherwise. Then the probability that each pulse is detected is given by

$$f_P(0, \tau_w)[f_P(0, \tau_w) + f_P(1, \tau_w)] = (1 + r\tau_w)\exp(-2r\tau_w), \quad (40)$$

which predicts the output count rate to be

$$n = r(1 + r\tau_w)\exp(-2r\tau_w).$$

Similarly, the probability that each pulse is detected for the general case of the allowed pile-up levels L is given by

$$f_P(0, \tau_w)\sum_{l=0}^{L-1} f_P(l, \tau_w) = \exp(-2r\tau_w)\sum_{l=0}^{L-1}(r\tau_w)^l/l!, \quad (41)$$

and the output count rate is given by

$$n = r\exp(-2r\tau_w)\sum_{l=0}^{L-1}(r\tau_w)^l/l!, \quad (42)$$

where the level L is normalized to the single-pulse-height level.

APPENDIX *B*
Scheme for constructing an approximate formula

Let us examine the formula

$$n = f_0(r; t) = t^{-1}[\exp(-rt) - \exp(-2rt)], \quad (43)$$

which is equivalent to the quadratic equation for $X = \exp(-rt)$,

$$X^2 - X + nt = 0. \quad (44)$$

The solution is immediately given by

$$X = \exp(-rt) = [1 + (1 - 4nt)^{1/2}]/2, \quad (45)$$

$$r = -t^{-1}\ln\{[1 + (1 - 4nt)^{1/2}]/2\}. \quad (46)$$

Since the first, second and third derivatives of the formula at the origin are given by

$$(dn/dr)_0 = 1, \quad (47)$$

$$(d^2n/dr^2)_0 = -3t, \quad (48)$$

$$(d^3n/dr^3)_0 = 7t^2, \quad (49)$$

the formula becomes comparable to the non-extended and extended dead-time models for $t = 2\tau/3$, which gives

$$(d^2n/dr^2)_0 = -2\tau, \quad (50)$$

$$(d^3n/dr^3)_0 = 28\tau^2/9. \quad (51)$$

It is suggested that the formula is close to the extended dead-time model but slightly deviated, to have a weak non-extended character, because the value $28\tau^2/9$ is close to but slightly greater than the third derivative of the extended model $3\tau^2$, while that of the non-extended dead-time model is given by $6\tau^2$.

It is also suggested that the extended dead-time model can be approximated by mixing the formulae of the non-extended dead-time model, if a negative value of the dead-time parameter for the non-extended component is allowed. We assume a mixed function as

$$f(r; t_1, t_2) = f_0[f_{\text{non-ex}}(r; t_1); t_2], \quad (52)$$

$$f_0(r; t_2) = t_2^{-1}[\exp(-rt_2) - \exp(-2rt_2)]. \quad (53)$$

The first, second and third derivatives of the mixed function at the origin are given by

$$f'(0; t_1, t_2) = 1, \quad (54)$$

$$f''(0; t_1, t_2) = -2t_1 - 3t_2, \quad (55)$$

$$f'''(0; t_1, t_2) = 7t_2^2 + 18t_1t_2 + 6t_1^2. \quad (56)$$

Substituting the solution of $f''(0; t_1, t_2) = -2\tau$ for t_1 in equation (56) gives

$$f'''(0; t_1, t_2) = 6\tau^2 - 13t_2^2/2. \quad (57)$$

The first, second and third derivatives of the mixed function at the origin then become identical to those of the extended dead-time model for $t_2 = (6/13)^{1/2}\tau$. When we introduce another parameter, ρ, to satisfy the relation

$$t_2 = (6\rho/13)^{1/2}\tau,$$

the third derivative of the mixed function becomes linearly dependent on ρ.

The present study was financially supported by the Nippon Sheet Glass Foundation for Materials Science and Engineering. The authors are indebted to the staff of the Photon Factory for their aid and for making the facilities available.

References

Chipman, D. R. (1969). *Acta Cryst.* A**25**, 209–219.
Cousins, C. S. G. (1994). *J. Appl. Cryst.* **27**, 159–163.
Müller, J. W. (1973). *Nucl. Instrum. Methods*, **112**, 47–57.
Omote, K. (1990). *Nucl. Instrum. Methods Phys. Res. Sect. A*, **293**, 582–588.
Quintana, J. P. (1991). *J. Appl. Cryst.* **24**, 261–262.
Reed, S. J. B. (1972). *J. Phys. E*, **5**, 994–996.
Toraya, H., Hibino, H. & Ohsumi, K. (1996). *J. Synchrotron Rad.* **3**, 75–83.